JCIM JOURNAL OF CHEMICAL INFORMATION AND MODELING

Quantum Machine Learning Algorithms for Drug Discovery Applications

Kushal Batra, Kimberley M. Zorn, Daniel H. Foil, Eni Minerali, Victor O. Gawriljuk, Thomas R. Lane, and Sean Ekins*

Cite This: *J. Chem. Inf. Model.* 2021, 61, 2641−2647 Read Online

ACCESS | Metrics & More | Article Recommendations | Supporting Information

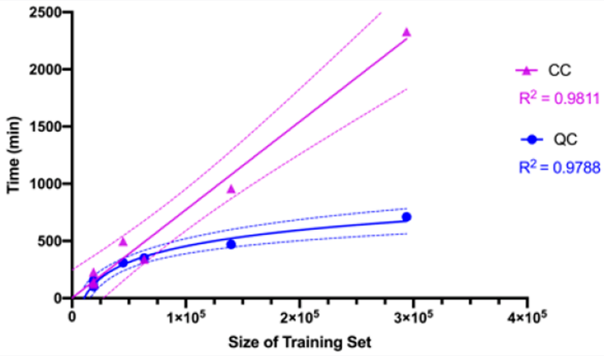

ABSTRACT: The growing quantity of public and private data sets focused on small molecules screened against biological targets or whole organisms provides a wealth of drug discovery relevant data. This is matched by the availability of machine learning algorithms such as Support Vector Machines (SVM) and Deep Neural Networks (DNN) that are computationally expensive to perform on very large data sets with thousands of molecular descriptors. Quantum computer (QC) algorithms have been proposed to offer an approach to accelerate quantum machine learning over classical computer (CC) algorithms, however with significant limitations. In the case of cheminformatics, which is widely used in drug discovery, one of the challenges to overcome is the need for compression of large numbers of molecular descriptors for use on a QC. Here, we show how to achieve compression with data sets using hundreds of molecules (SARS-CoV-2) to hundreds of thousands of molecules (whole cell screening data sets for plague and *M. tuberculosis*) with SVM and the data reuploading classifier (a DNN equivalent algorithm) on a QC benchmarked against CC and hybrid approaches. This study illustrates the steps needed in order to be "quantum computer ready" in order to apply quantum computing to drug discovery and to provide the foundation on which to build this field.

■ INTRODUCTION

The rapidly growing public and private data sets that are focused on small molecules screened against known biological targets or whole organisms[1] provide a wealth of data to facilitate drug discovery. Increasingly, this is used to create machine learning models[2] which can be used for enabling target-based design,[3−5] predicting on- or off-target effects, and creating scoring functions.[6,7] The pharmaceutical industry and academic laboratories are increasingly using and exploring machine learning applications in drug discovery to mine and model their data generated from years of high throughput screening.[8] This is allowing rapid identification of molecules for neglected diseases such as Ebola[9] and Chagas disease,[10] presenting lead compounds which can then be moved rapidly into *in vivo* models,[11−13] and this approach can be more widely applied in cheminformatics. Recent examples have illustrated the speed with which the machine learning combined with *in vitro* testing continuum can generate new leads compared to traditional efforts.[14] The availability of thousands of structure−activity data sets (some of which in turn contain data for hundreds of thousands of molecules screened against a single target or organism[2,15]) presents a computational challenge with machine learning methods such as classifiers like support vector machines (SVM) on a classical computer (CC).[16]

Recently, the potential of quantum machine learning has been illustrated using two methods such as a variational quantum circuit and a quantum kernel estimator.[17] In addition, new machine learning methods for quantum computing continue to be developed[18,19] which creates opportunities to expand the possible applications of machine learning to drug discovery and toxicology. Like many emerging technologies, the quantum computer (QC) has been proposed as likely to transform early stage pharmaceutical research and development as well as provide a potential solution for data sets that would be intractable if performed on a CC.[20,21] One area of interest in early drug discovery is in cheminformatics for virtual screening and optimization, where small molecules are frequently described by fingerprint descriptors which can lead to tens of thousands of vectors called multiple fingerprint features (MFF).[22] While this may be important for many aspects of applying machine learning to chemistry,[23] it also creates significant challenges when using these massive numbers of

Received: February 12, 2021
Published: May 25, 2021

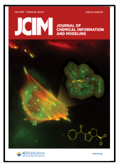

ACS Publications

https://doi.org/10.1021/acs.jcim.1c00166

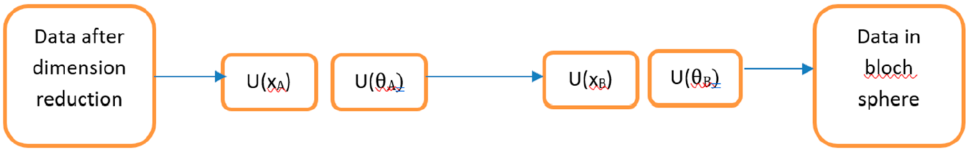

Figure 1. A high-level abstraction of how data are stored in the bloch sphere. The two layers—A and B, with $U(x_A)$ denoting unitary applied on the input vector, $U(\theta_A)$ representing the unitary applied to rotate the vector in the bloch sphere.

descriptors on a QC. This is mainly because we do not have enough resources and techniques to represent compounds with such large descriptors on QCs as the system will collapse.

Herein, we describe how we have applied multiple approaches to compress the descriptors for QC while also demonstrating applications to drug discovery data sets on a range of scales that would be broadly applicable for drug discovery. We also describe hybrid approaches that merge QC with CC for machine learning applied to these data sets curated from public sources. These include 132 small molecule inhibitors of SARS-CoV-2 in Vero cells[24] and 18 886 inhibitors of *Mycobacterium tuberculosis*[25] as well as several larger data sets for inhibitors of Krabbe disease (β-galactocerebrosidase, Pubchem Assay 1159614, 44 809 compounds), cathepsin B (Pubchem Assay 453, 63 331 compounds), plague (*Yersinia pestis*, Pubchem Assay 898, 139 861 compounds), a second much larger data set for *M. tuberculosis* (293 937 compounds),[26] and hERG (306 587 compounds).[15] All these data sets were curated and prepared using Assay Central[25] (see Methods), and the models can be applied for predicting new molecules for these targets or diseases.

■ METHODS

Experimental Procedures. *Data Curation.* Our proprietary Assay Central software[27,28] is a framework for curating high-quality data sets and building Bayesian machine learning models. Each data set was subjected to the same standardization processes (i.e., removing salts, metal complexes and mixtures) prior to building models. Duplicate parent compounds with finite concentration activities are merged into a single entry. Classification models such as these require a defined threshold of bioactivity. The SARS-CoV-2 model used a threshold of 6.65 μM; cathepsin B used >20% inhibition. The three *M. tuberculosis* models used the thresholds as described; the Krabbe model used actives defined by the authors. Plague used a threshold at ≥50% inhibition; the hERG central data set was >50% inhibition. The large *M. tuberculosis* model used a cutoff where MIC_{90} or IC_{90} < 10 μg/mL or 10 μM and a selectivity index (SI) greater than 10 was used (where SI = MIC_{90} or IC_{90}/CC_{50}).[26] The curated files that were output from Assay Central were then employed for quantum machine learning.

Running Our Algorithms on QC. We used IBM's ibmq_rochester for executing our algorithms. Figure S1 shows the architecture of ibmq_rochester. Colors represent error probabilities for controlled-NOTs and readout on qubits.[29] This architecture has 53 qubits linked in the network. These 53 qubits are assembled and connected following the property of hexagonal lattices, which is advantageous when it comes to minimizing unwanted interactions (Figure S1).[29] The error in reporting the accuracies can be ±3% depending on the time of day the code is run due to their recalibration. The QC is recalibrated once a day at unknown times. The algorithm was run with shots = 2048.

Descriptor Compression for Quantum Machine Learning of SARS-CoV-2 Data. As the extended connectivity fingerprint diameter 6 (ECFP6) has been widely applied in cheminformatics,[27] we used the Morgan Fingerprint (with radius 3), which is equivalent to the ECFP6 fingerprint in RDkit.[30] The Morgan Fingerprint generates binary numbers whose default size is 2048 bits. While this is acceptable for use on a CC, it is not acceptable for use on a QC as 2048 bits exceeds the maximum capacity of current state-of-technology gate-based QCs. Apart from this, having a relatively big descriptor size, around 1000, can also be a challenge. This is because with the increase in size/usage of qubits on the QC network, to represent descriptors, accuracy fails because of decoherence noise introduced in the qubit system.[31] Depending on the architecture of QC being used, it is possible that not all qubits are linked with each other. Having no linkage or communication between every qubit adds further noise to this system. We attempted two approaches to solve this utilizing QC alone or a hybrid where part of the code is run on the QC.

We propose four methods (utilizing QC alone or a hybrid where part of the code is run on the QC) to encode the 2048 descriptor features. Method 1 used principal component analysis (PCA) that is widely applied in data compression.[32] Method 2 used a common dimension reduction technique of linear discriminant analysis (LDA), which also considers the target class along with the predictors.[33] In this, we simply take a projection of points into some other hyperplane. In method 3, we designed an algorithm where first we divide the 2048 molecule fingerprint bits into "*x*" groups, such that, each group has "*k*" bits. This means that *k* should divide 2048 completely with 0 as the remainder. These "*k*" bits are then converted into base 10 or a decimal value. This process is repeated until all the groups are converted to a decimal. Method 4 uses an algorithm where we keep track of positions of 1 in the whole array.

Another approach we have applied is a hybrid approach in which the QC is used to perform part of the calculation while performing the remainder on a CC. This removes the storage limitation on QC as this is provided by the CC, hence leaving the processing to the QC. A data reuploading classifier was used as described further below.[34] Here, unlike SVM where we were reducing to two to three dimensions, we can reduce to three to 10 dimensions to consider the qubit architecture. For our purpose, we reduced to six dimensions using method 1 and method 3 for SVM. In this approach, we load data into a single qubit by performing a simple unitary operation $U(x1, x2, x3)$ where $x1$, $x2$, and $x3$ are the coordinates of the point. When dimensions are greater than three, we can have $U(x1, x2, x3, x4, x5, x6)$ to $(U(x1, x2, x3), U(x4, x5, x6))$. Using this approach, we can therefore store a data point which has six dimensions. We can have a similar unitary $U(\theta_1, \theta_2, \theta_3)$ for rotation of data point in the bloch sphere (Figure 1). Here, we make a two-qubit connected layer to introduce nonlinearity in our network.

The hybrid algorithm helps in introducing nonlinearity to the model which makes use of the Adam stochastic gradient

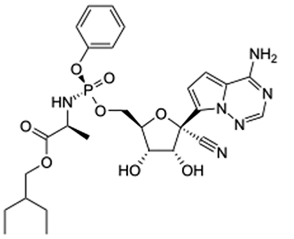

An example: Take k= 128 bits (as 2048 completely divided by 128)

For Remdesivir ECPF6 =

```
[01000001000000000000000010000000010010000001011000000000000000001000000000000000100
000000000000000000000000000001000001000000000100000000000000000000100000000000000000000
0000000000000000000000000100000000000000000000000000000000000000001000000000000000000
000000000000000000000000000000001000000000010000000000000000000000000001000000000000
000000000000000000000100010000000000000000010000000000000000010000000000000001000100
000000000100001010000000000000000000000000001000000000000000000000001001000000000000000
000000000000000001000000000000000000000000000000000000000000000000000000000000000000
000000000000000000000001000000000000000100000000000000000000000100000100000000000000
000100000000000000000100100000000000000000000000000000100000000000000000000000000000
000000000000100000000000000000000001000000000000000010000000000000000000000000000000
000000000010000000000000000000000000000000000000000001000000000000000000000000000000
000001000000100000000000000000000000000000000000000000000000010000000000000000
00000000000010000]
```

Using the above algorithm, we get the following compressed output =
[4683744163430531072, 9223512774343164416, 9223389629040820224, 9223372036858970112, 68753031168, 2305843009356300320, 2251836321452032, 281475014459392, 36028797018963968, 536879104, 9147937279969536, 2199023255553, 2199040032768, 70368744177668, 2164260864, 17179869200]

Figure 2. An example of a molecule and its compression using the Method 3.2D representation of the antiviral Remdesivir and an illustration of the ECFP6 descriptor for Remdesivir and the compressed output.

optimizer.[35] We tuned different parameters using an iterative process for the following: optimizer (Adagrad and Adam), epochs, batch size, and the number of hidden layers.

The CC Details on Which the Algorithms Were Executed. The computational server used was a Supermicro EATX DDR4 LGA 2011, Intel Computer CPU 2.1 8 BX80660E52620 V4, Crucial 64 GB Kit (16GBx4) DDR4 2133 (PC42133) DR x4 288 Pin Server Memory CT4K16G4RFD4213/CT4C16G4RFD4213, 1−5 x EVGA GeForce GTX 1080 Ti FOUNDERS EDITION GAMING, 11 GB GDDR5X, Intel 730 SERIES 2.5 Inch Solid State Drive SSDSC2BP480G410, WD Gold 4TB Datacenter Hard Disk Drive 7200 rpm Class SATA 6 Gb/s 128 MB Cache 3.5 Inch WD4002FYYZ, Supermicro 920 W 4U Server.

Quantum SVM. The initial algorithm we have compared is an SVM implemented using the Qiskit library,[36] which uses least-square SVM (LS-SVM).[37] Qiskit chooses $M_{ij} = x_i x_j$ as the ansatz where M_{ij} is the kernel matrix and $x_i x_j$ are the data points in the data set.[38] When working with QC, we first formulate the ansatz and try to minimize it. This ansatz formulates the SVM hyperplane which divides the data sets. We have chosen the ansatz such that we get a line as output. The main reason we selected linear fit and not polynomial fit is because we wanted to avoid the scenario of nonconvergence kernels. This ansatz equation determines the shape the hyperplane will take. We made use of already available QSVM (Quantum SVM) code available in the Qiskit library. For the data set, the SVM's depth was set to 2. Entanglement was set to "full," and the skip_qobj_validation parameter for quantum instance was set to false.

Data Reuploading Classifier. The MFF molecular descriptor[22] was also used with the four methods to achieve better accuracy rates. The data reuploading classifier is very similar to a deep neural network (DNN),[34] implemented using the existing library in the Pennylane tool,[39] where a single qubit represents a neural network layer. A DNN consists of two or more hidden layers. So, to replicate the DNN properties and introduce nonlinearity, we make use of 2 qubits as an analogy to two-layer neural networks. With the above MFF descriptor, we get 71 375 vectors. Sandfort et al.[22] postulated that this leads to overfitting, and the same results were observed with MFF followed by our data reduction algorithm. For all data sets in this study, the data reuploading classifier had hyperparameters set to training set size, 70% of data set; test set size, 30% of data set; train accuracy rate, 61.2%; test accuracy rate, 61%; number of layers, 4; batch size, 32; epochs, 10; optimizer, Adam; learning rate, 0.6; cross fold validation, 5.

■ RESULTS

Descriptor Compression for Quantum Machine Learning of SARS-CoV-2 Data. Within the QC, a quantum algorithm is used to solve the direct product[37] to solve for matrix operations and then calculate the **M** (the kernel matrix). Then, a quantum algorithm can be used to transform into waveforms to solve the system of linear equations.[38] This approach solves the complete SVM on a QC. While SVM generally provides promising results, it takes considerable time to solve linear equations to solve for the kernel matrix using feature maps (1.24 min for each data point), and hence, any time advantage for QC is likely not achievable. It should be noted that the connection to the qubit architecture also plays an instrumental role in driving the accuracy rates which may vary slightly for the best accuracy value. The accuracy rates reported are therefore a best value achieved on the QC or QC simulator.

In order to reduce the molecular descriptor features such that they can be represented and stored in our limited number of qubits (53 qubits for the ibmq-rochester, Figure S1). We have initially demonstrated the application of QC with a SARS-CoV-2 Vero cell inhibition data set consisting of 132 compounds, of which 66 were found to be active with the IC_{50} activity threshold of 6.65 μM, which was selected using our Assay Central software.[24] We reduced the molecular descriptor dimensions from 2048 descriptor features to two to three using multiple techniques. Method 1 (i.e., PCA) resulted in accuracy rates on a CC with 1 GPU of 37% using the kernel algorithm RBF (radial basis function), whereas on a QC, accuracy was 33% (N = 3). Method 2 (i.e., LDA) resulted in accuracy rates of 40% using a kernel algorithm on a CC, while on a QC this was 39% (N = 3). An example of a molecule compressed using method 3 is shown in Figure 2. Method 3 resulted in a greatly improved accuracy rate of 61% on a CC using kernel algorithm = "poly'" and 59.6% on a QC (n = 3).

Applying method 4 using the same example of Remdesivir, we get two values [−21086, −502690], where −21086 is storing the positions of 1's and −502690 is storing the positions of 0's. Using this approach, we get two dimensions that can be easily fed into the model. All the algorithms discussed above try to retain most of the information from the molecular descriptors as much as possible. This resulted in accuracy rates on the CC of 59% using kernel algorithm = "sigmoid" and on the QC of 59.25% (with n = 2).

These four methods were implemented on the QC and then tried as combinations, and the accuracy was compared with the CC (Table 1). The most promising results were obtained when combining method 1 and method 3 (k = 128). The improved results for k = 128 are due to the increased spread (more variance) as compared to other k values when combined with PCA (Figure 3). This makes it easier to obtain a hyperplane separating the two classes (active or not active). The Kernel matrix obtained from running the SVM model on a QC is shown in Figure 4.

Table 1. Accuracy Rates Achieved with Different Combinations of Methods[a]

Combination	Accuracy on QC (%)	Accuracy on CC (%)
PCA + Method 3(k = 64)	<30	47
PCA + Method 3(k = 128)	62.9	65
PCA + Method 3(k = 256)	59.25	60
PCA + Method 3(k = 512)	41	44
LDA + Method 3(k = 64)	31	36
LDA + Method 3(k = 128)	<30	35
LDA + Method 3(k = 256)	<30	31
LDA + Method 3(k = 512)	32	59
PCA + Method 4(2)	59.25	60
LDA + Method 4(2)	57	57

[a] Method 1 (PCA), method 2 (LDA), method 3, and method 4 using SVM on the classical and the quantum computer.

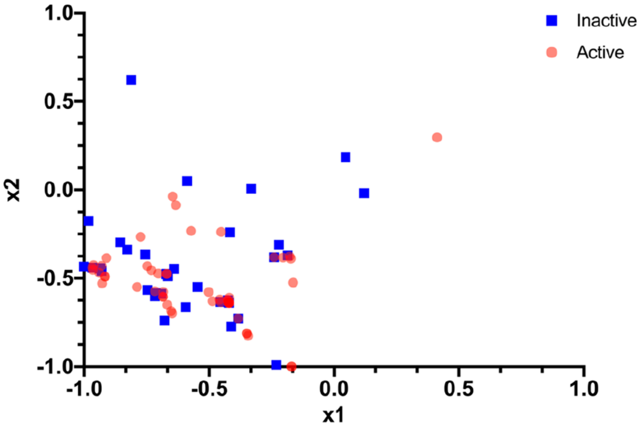

Figure 3. Spread of the data for the SARS-CoV-2 data set after applying method 1 and method 3. "x1" and "x2" are the top two features respectively (for all the compounds) obtained after applying these two methods.

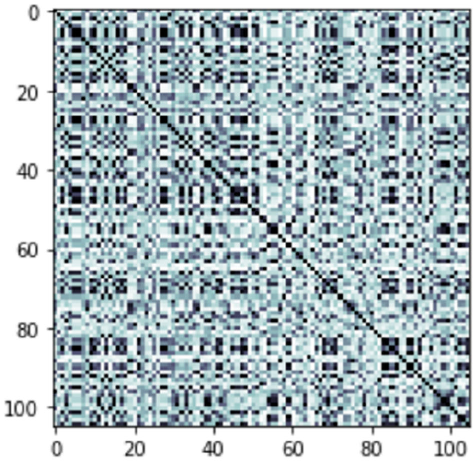

Figure 4. Kernel matrix obtained using PCA and method 3 for the SARS-CoV-2 data set.

Another approach we have applied is a hybrid approach (i.e., QC performs part of the calculation and CC, the remainder) to remove the storage limitation on QC. We reduced the data point to six dimensions using method 1 and method 3 for SVM. We loaded data into a single qubit by performing a simple unitary operation $U(x1, x2, x3)$ where $x1$, $x2$, and $x3$ are the coordinates of the point. When dimensions are greater than three, we can have $U(x1, x2, x3, x4, x5, x6)$ to $(U(x1, x2, x3), U(x4, x5, x6))$. We have a similar unitary $U(\theta_1, \theta_2, \theta_3)$ for rotation of data points in the bloch sphere (Figure 4) to make a two-qubit connected layer. For the same SARS-CoV-2 data set, we obtained accuracy rates of 61%.

Applications of Quantum Machine Learning to M. tuberculosis Data Sets. The same hybrid algorithm was then implemented on *M. tuberculosis* data sets, which were representative of high throughput screening data (i.e., tens of thousands of compounds). For all of these data sets, we applied method 1 and method 3 for reducing the dimension and feeding it into our data reuploading classifier as well as for plotting and visualization purposes. We also worked with the MFF descriptors,[22] which generated a 71 375-descriptor vector. Data sets for *in vitro* inhibitors of *M. tuberculosis* had three variants, namely, with a cutoff at of 100 nM, 1 μM, and 10 μM.[25] Figure 5 shows a plot for the 100 nM cutoff *M. tuberculosis* data set when we reduced it into two dimensions.

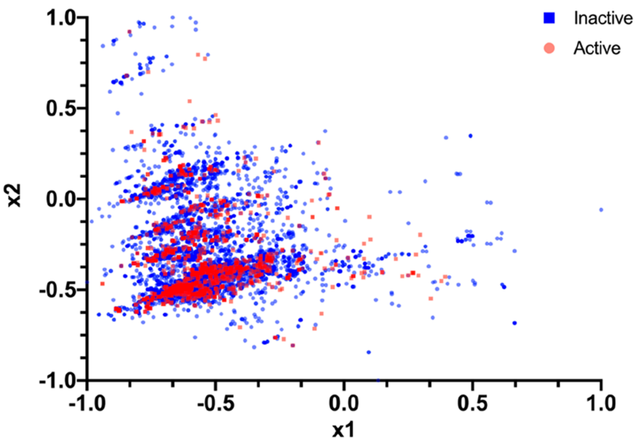

Figure 5. A 2D plot representing the spread of data for the *M. tuberculosis* (100 nM) data set. This takes the important features using dimension = 2 instead of 6. "x1" and "x2" are the top two features, respectively (for all the compounds), that have been calculated using method 1 and method 3.

For these three data sets, the data reuploading classifier was run and then compared with the results obtained with CC (Table 2, Table S1). In Table 2, we see that the accuracy obtained on a QC is closer to that obtained on a CC with a slight time advantage over CC, such that there is a trade-off of accuracy and speed with these data sets. All of the above-reported data are implemented on a QC (ibmq_rochester).

Table 2. Comparing Accuracy and Run Time Results for *M. tuberculosis* Inhibition Datasets (18,886 Compounds)[25] Using the Data Reuploading Classifier on CC with Three GPUs versus QC with 5-Fold Cross-Validation Using SVM

data set threshold (number of actives)	time on CC (min)	CC accuracy (%)	time on QC (min)	QC accuracy (%)
100 nM (645)	125	97.1	104	90.5
1 mM (2351)	144	90.4	101	81.4
10 mM (7762)	229	75.6	153	54.9

Applications of Quantum Machine Learning to Large in Vitro Data Sets. The data reuploading classifier algorithm[34] was implemented with the ECFP6 molecular descriptor and tested with five considerably larger drug discovery data sets ranging from 44 000−293 000 molecules on a QC simulator (Table 3). Running them on a QC with the transfers of data was the major overhead here for such large data sets. We find that the results obtained are very comparable with a slight time advantage for the QC simulator over CC. The linearity of calculation time on a CC with data set size was apparent, and this plateaued for the QC simulator (Figure 6).

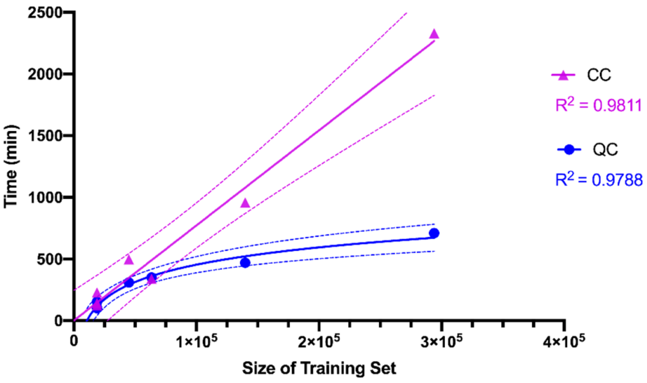

Figure 6. Comparing data set size with run time for quantum computer (QC) simulator and classical computer (CC). Linear or nonlinear (semilog) fit lines for the data generated. These show that the likely relationship of CC and QM model sizes versus calculation time is on a linear and semilog scale, respectively. The dotted lines represent the 99% confidence bands of these lines to highlight the likelihood of this relationship.

■ DISCUSSION

We have discussed four approaches and their combination for compression of the molecular descriptors, followed by calculation of the machine learning model on a QC. We found that the results were optimal when combining method 3 and method 1, most likely due to the increased spread of data after employing these techniques. Further, we applied both the QC and hybrid approach to train our model. With the current QC hardware available, the option of choosing the hybrid approach for drug discovery is likely optimal. When dealing with bigger *in vitro* structure−activity data sets on the order of tens of thousands of molecules, we found that the data communication overhead between computer and cloud-based QC was much larger than the actual time taken for a circuit to execute on QC. Plotting the time versus size of a data set for CC vs QC simulator also suggests the likely potential speed of model building on a QC with larger data sets if we are able to replicate the same settings on a QC (Figure 6). Now that we have optimized these steps for machine learning, we have demonstrated that QC can handle "very large" drug discovery

Table 3. Comparing Large Scale Drug Discovery Datasets on a Quantum Computer Simulator and CC with Five GPUs for Data Reuploading Classifier Using the ECFP6 Descriptor Obtained from Method 1 and Method 2[a]

		QC			CC	
data set target	total compounds (active)	training accuracy (%)	testing accuracy (%)	time on QC (min/epoch)	training accuracy (%)	time on CC (min)
cathepsin B	63 331 (75)	99.4	99.1	35 (10 epochs)	99.8	341.25
Krabbe disease	44 809 (63)	91.2	92.4	31 (10 epochs)	99.9	497.91
plague	139 861 (223)	92.9	93.1	47 (10 epochs)	99.8	958.59
M. tuberculosis	293 937 (6104)	90.4	91.3	71 (10 epochs)	97.9	2329.4
hERG	306 587 (233)	82.7	82.5	313 (ran for 5 epochs)	ND	ND

[a] Algorithms on QC Simulator were run for 10 epochs with 5-fold crossvalidation unless noted. ND = not determined.

data sets on the order of hundreds of thousands of molecules. At the time of this work, data for SARS-CoV-2 available for machine learning were in the hundreds of molecules, and now they are likely in the low thousands of molecules.[24] Yet, such data sets clearly do not require the performance of QC. However, the larger high-throughput screening data sets for other targets and diseases that have been amassing in public databases like PubChem[40] and ChEMBL[1] present significant challenges for SVM and deep neural networks as well as other computationally intensive tools. QC is therefore a viable approach to overcoming some of these limitations and allowing practical computing times. With thousands of such data sets now readily available, being able to curate and update them quickly will be important as new screening data are added. Obviously, as we start to see DNA encoded libraries with sizes in the millions to possibly billions of molecules being used for generating high throughput screening data, then we will likely need QC for machine learning with algorithms that are computation intensive in order to see results in a reasonable time. This study demonstrates the nonlinear scaling of compute time on a QC with multiple independent data sets of different sizes, compared with the linearity observed on a CC. As quantum machine learning develops, the accessibility of QC will increase for drug discovery cheminformatics applications as we have demonstrated here. Future studies to evaluate these and other quantum machine learning models will also need to involve prospective prediction and experimental validation in order to provide convincing evidence of their value for drug discovery.

■ ASSOCIATED CONTENT

Supporting Information

The Supporting Information is available free of charge at https://pubs.acs.org/doi/10.1021/acs.jcim.1c00166.

> A supplemental figure describing the IBM Rochester architecture map and a supplemental table describing the large tuberculosis data set model confusion tables (PDF)

■ AUTHOR INFORMATION

Corresponding Author

Sean Ekins − *Collaborations Pharmaceuticals, Inc., Raleigh, North Carolina 27606, United States;* orcid.org/0000-0002-5691-5790; Phone: 215-687-1320; Email: sean@collaborationspharma.com

Authors

Kushal Batra − *Computer Science, North Carolina State University, Raleigh, North Carolina 27606, United States*
Kimberley M. Zorn − *Collaborations Pharmaceuticals, Inc., Raleigh, North Carolina 27606, United States*
Daniel H. Foil − *Collaborations Pharmaceuticals, Inc., Raleigh, North Carolina 27606, United States*
Eni Minerali − *Collaborations Pharmaceuticals, Inc., Raleigh, North Carolina 27606, United States*
Victor O. Gawriljuk − *São Carlos Institute of Physics, University of São Paulo, São Carlos, São Paulo 13563-120, Brazil*
Thomas R. Lane − *Collaborations Pharmaceuticals, Inc., Raleigh, North Carolina 27606, United States*

Complete contact information is available at: https://pubs.acs.org/10.1021/acs.jcim.1c00166

Author Contributions

S.E. led the project and designed experiments. K.B. performed work on the descriptor compression and algorithm comparisons. K.M.Z, D.H.F., E.M., T.R.L., and V.O.G. curated the data sets. T.R.L. provided graphics. All authors contributed to the manuscript.

Notes

The authors declare the following competing financial interest(s): S.E., K.M.Z., D.H.F., E.M., and T.R.L. work for Collaborations Pharmaceuticals, Inc. K.B. and V.O.G. have no conflicts of interest.

■ ACKNOWLEDGMENTS

Professor Daniel D. Stancil (NC State) is kindly acknowledged for his helpful guidance and for quantum computing and overall support of this project. Access to the IBM Q Network was obtained through the IBM Q Hub at NC State. We gratefully acknowledge our many colleagues and collaborators who assisted in curating these datasets used as examples for this study as well as Mr. Valery Tkachenko for hardware support and Dr. Alex M. Clark for Assay Centralsupport. We kindly acknowledge NIH funding to develop the software from R44GM122196-02A1 “Centralized assay datasets for modelling support of small drug discovery organizations” and from NIGMS and NIEHS for 1R43ES031038-01 “MegaTox for analyzing and visualizing data across different screening systems.” Research reported in this publication was supported by the National Institute of Environmental Health Sciences of the National Institutes of Health under Award Number R43ES031038. The content is solely the responsibility of the authors and does not necessarily represent the official views of the National Institutes of Health. V.O.G. was supported by FAPESP funding: 2019/25407-2. All data sets and software are available from the author upon written request.

■ ABBREVIATIONS

CC, classical computer; DNN, deep neural networks; ECFP6, extended connectivity fingerprint radius 6; LDA, linear discriminant analysis; MFF, multiple fingerprint features; PCA, principal component analysis; QC, quantum computer; SVM, support vector machines

■ REFERENCES

(1) Gaulton, A.; Hersey, A.; Nowotka, M.; Bento, A. P.; Chambers, J.; Mendez, D.; Mutowo, P.; Atkinson, F.; Bellis, L. J.; Cibrian-Uhalte, E.; Davies, M.; Dedman, N.; Karlsson, A.; Magarinos, M. P.; Overington, J. P.; Papadatos, G.; Smit, I.; Leach, A. R. The ChEMBL database in 2017. *Nucleic Acids Res.* **2017**, *45*, D945−D954.

(2) Lane, T. R.; Foil, D. H.; Minerali, E.; Urbina, F.; Zorn, K. M.; Ekins, S. Bioactivity Comparison across Multiple Machine Learning Algorithms Using over 5000 Datasets for Drug Discovery. *Mol. Pharmaceutics* **2021**, *18*, 403−415.

(3) Bosc, N.; Atkinson, F.; Felix, E.; Gaulton, A.; Hersey, A.; Leach, A. R. Large scale comparison of QSAR and conformal prediction methods and their applications in drug discovery. *J. Cheminf.* **2019**, *11*, 4.

(4) Nogueira, M. S.; Koch, O. The Development of Target-Specific Machine Learning Models as Scoring Functions for Docking-Based Target Prediction. *J. Chem. Inf. Model.* **2019**, *59*, 1238−1252.

(5) Imrie, F.; Bradley, A. R.; van der Schaar, M.; Deane, C. M. Protein Family-Specific Models Using Deep Neural Networks and Transfer Learning Improve Virtual Screening and Highlight the Need for More Data. *J. Chem. Inf. Model.* **2018**, *58*, 2319−2330.

(6) Shaikh, N.; Sharma, M.; Garg, P. An improved approach for predicting drug-target interaction: proteochemometrics to molecular docking. *Mol. BioSyst.* **2016**, *12*, 1006−14.

(7) Mayr, A.; Klambauer, G.; Unterthiner, T.; Steijaert, M.; Wegner, J. K.; Ceulemans, H.; Clevert, D. A.; Hochreiter, S. Large-scale comparison of machine learning methods for drug target prediction on ChEMBL. *Chem. Sci.* **2018**, *9*, 5441−5451.

(8) Ekins, S.; Puhl, A. C.; Zorn, K. M.; Lane, T. R.; Russo, D. P.; Klein, J. J.; Hickey, A. J.; Clark, A. M. Exploiting machine learning for end-to-end drug discovery and development. *Nat. Mater.* **2019**, *18*, 435−441.

(9) Ekins, S.; Freundlich, J. S.; Clark, A. M.; Anantpadma, M.; Davey, R. A.; Madrid, P. Machine learning models identify molecules active against the Ebola virus in vitro. *F1000Research* **2015**, *4*, 1091.

(10) Ekins, S.; Lage de Siqueira-Neto, J.; McCall, L.-I.; Sarker, M.; Yadav, M.; Ponder, E. L.; Kallel, E. A.; Kellar, D.; Chen, S.; Arkin, M.; Bunin, B. A.; McKerrow, J. H.; Talcott, C. Machine Learning Models and Pathway Genome Data Base for Trypanosoma cruzi Drug Discovery. *PLoS Neglected Trop. Dis.* **2015**, *9*, No. e0003878.

(11) Lane, T. R.; Massey, C.; Comer, J. E.; Anantpadma, M.; Freundlich, J. S.; Davey, R. A.; Madrid, P. B.; Ekins, S. Repurposing the antimalarial pyronaridine tetraphosphate to protect against Ebola virus infection. *PLoS Neglected Trop. Dis.* **2019**, *13*, No. e0007890.

(12) Lane, T. R.; Comer, J. E.; Freiberg, A. N.; Madrid, P. B.; Ekins, S. Repurposing Quinacrine Against Ebola Virus Infection In vivo. *Antimicrob. Agents Chemother.* **2019**, *63*, No. e01142-19.

(13) Ekins, S.; Lingerfelt, M. A.; Comer, J. E.; Freiberg, A. N.; Mirsalis, J. C.; O'Loughlin, K.; Harutyunyan, A.; McFarlane, C.; Green, C. E.; Madrid, P. B. Efficacy of Tilorone Dihydrochloride against Ebola Virus Infection. *Antimicrob. Agents Chemother.* **2018**, *62*, No. e01711-17, DOI: 10.1128/AAC.01711-17.

(14) Zhavoronkov, A.; Ivanenkov, Y. A.; Aliper, A.; Veselov, M. S.; Aladinskiy, V. A.; Aladinskaya, A. V.; Terentiev, V. A.; Polykovskiy, D. A.; Kuznetsov, M. D.; Asadulaev, A.; Volkov, Y.; Zholus, A.; Shayakhmetov, R. R.; Zhebrak, A.; Minaeva, L. I.; Zagribelnyy, B. A.; Lee, L. H.; Soll, R.; Madge, D.; Xing, L.; Guo, T.; Aspuru-Guzik, A. Deep learning enables rapid identification of potent DDR1 kinase inhibitors. *Nat. Biotechnol.* **2019**, *37*, 1038−1040.

(15) Du, F.; Yu, H.; Zou, B.; Babcock, J.; Long, S.; Li, M. hERGCentral: a large database to store, retrieve, and analyze compound-human Ether-a-go-go related gene channel interactions to facilitate cardiotoxicity assessment in drug development. *Assay Drug Dev. Technol.* **2011**, *9*, 580−8.

(16) Nalepa, J.; Kawulok, M. Selecting training sets for support vector machines: a review. *Artificial Intelligence Review* **2019**, *52*, 857−900.

(17) Havlicek, V.; Corcoles, A. D.; Temme, K.; Harrow, A. W.; Kandala, A.; Chow, J. M.; Gambetta, J. M. Supervised learning with quantum-enhanced feature spaces. *Nature* **2019**, *567*, 209−212.

(18) Fastovets, D. V.; Bogdanov, Y. I.; Bantysh, B. I.; Lukichev, V. F. Machine learning methods in quantum computing theory. https://arxiv.org/abs/1906.10175 (accessed April 9, 2021).

(19) Broughton, M.; Verdon, G.; McCourt, T.; Martinez, A. J.; Yoo, J. H.; Isakov, S. V.; Massey, P.; Niu, M. Y.; Halavati, R.; Peters, E.; Leib, M.; Skolik, A.; Streif, M.; Von Dollen, D.; McClean, J. R.; Boixo, S.; Bacon, D.; Ho, A. K.; Neven, H.; Mohseni, M. TensorFlow Quantum: A Software Framework for Quantum Machine Learning. https://arxiv.org/abs/2003.02989 (accessed April 9, 2021).

(20) Langione, M.; Bobier, J.-F.; Meier, C.; Hasenfuss, S.; Schulze, U. Will quantum computing transform biopharma R&D? https://www.bcg.com/publications/2019/quantum-computing-transform-biopharma-research-development.aspx (accessed April 9, 2021).

(21) Schuld, M. Machine learning in quantum spaces. *Nature* **2019**, *567*, 179−181.

(22) Sandfort, F.; Strieth-Kalthoff, F.; Kühnemund, M.; Beecks, C.; Glorius, F. A Structure-Based Platform for Predicting Chemical Reactivity. *Chem.* **2020**, *6*, 1379−1390.

(23) Pattanaik, L.; Coley, C. W. Molecular Representation: Going Long on Fingerprints. *Chem.* **2020**, *6*, 1204−1207.

(24) Gawriljuk, V. O.; Kyaw Zin, P. P.; Foil, D. H.; Bernatchez, J.; Beck, S.; Beutler, N.; Ricketts, J.; Yang, L.; Rogers, T.; Puhl, A. C.; Zorn, K. M.; Lane, T. R.; Godoy, A. S.; Oliva, G.; Siqueira-Neto, J. L.; Madrid, P. B.; Ekins, S., Machine Learning Models Identify Inhibitors of SARS-CoV-2. *bioRxiv* **2020**, 2020.06.16.154765. https://www.biorxiv.org/content/10.1101/2020.06.16.154765v1 (accessed April 9, **2021**).

(25) Lane, T.; Russo, D. P.; Zorn, K. M.; Clark, A. M.; Korotcov, A.; Tkachenko, V.; Reynolds, R. C.; Perryman, A. L.; Freundlich, J. S.; Ekins, S. Comparing and Validating Machine Learning Models for Mycobacterium tuberculosis Drug Discovery. *Mol. Pharmaceutics* **2018**, *15*, 4346−4360.

(26) Ekins, S.; Freundlich, J. S.; Reynolds, R. C. Are bigger data sets better for machine learning? Fusing single-point and dual-event dose response data for Mycobacterium tuberculosis. *J. Chem. Inf. Model.* **2014**, *54*, 2157−65.

(27) Clark, A. M.; Dole, K.; Coulon-Spektor, A.; McNutt, A.; Grass, G.; Freundlich, J. S.; Reynolds, R. C.; Ekins, S. Open Source Bayesian Models. 1. Application to ADME/Tox and Drug Discovery Datasets. *J. Chem. Inf. Model.* **2015**, *55*, 1231−45.

(28) Clark, A. M.; Ekins, S. Open Source Bayesian Models. 2. Mining a "Big Dataset" To Create and Validate Models with ChEMBL. *J. Chem. Inf. Model.* **2015**, *55*, 1246−60.

(29) Wootton, J. R. Benchmarking near-term devices with quantum error correction. https://arxiv.org/abs/2004.11037 (accessed April 9, 2021).

(30) Landrum, G. RDkit. https://www.rdkit.org (accessed April 9, 2021).

(31) Saki, A. A.; Alam, M.; Ghosh, S. Study of Decoherence in Quantum Computers: A Circuit-Design Perspective. https://arxiv.org/abs/1904.04323 (accessed April 9, 2021).

(32) Paul, L. C.; Suman, A. A.; Sultan, N. Methodological analysis of principal component analysis (PCA) method. *Int. J. Comp Eng. Management* **2013**, *16*, 32−38.

(33) Tharwat, A.; Gaber, T.; Ibrahim, A.; Hassanien, A. E. Linear discriminant analysis: A detailed tutorial. *AI Communications* **2017**, *30*, 169−190.

(34) Pérez-Salinas, A.; Cervera-Lierta, A.; Gil-Fuster, E.; Latorre, J. I. Data re-uploading for a universal quantum classifier. *Quantum* **2020**, *4*, 226.

(35) Kingma, D. P.; Ba, J. Adam: A method for stochastic optimization. https://arxiv.org/abs/1412.6980 (accessed April 9, 2021).

(36) Anon Qiskit: An Open-source Framework for Quantum Computing. https://github.com/Qiskit/qiskit/blob/master/Qiskit.bib (accessed April 9, 2021).

(37) Rebentrost, P.; Mohseni, M.; Lloyd, S. Quantum support vector machine for big data classification. *Phys. Rev. Lett.* **2014**, *113*, 130503.

(38) Abhijith, J.; Adedoyin, A.; Ambrosiano, J.; Anisimov, P.; Bärtschi, A.; Casper, W.; Chennupati, G.; Coffrin, C.; Djidjev, H.; Gunter, D.; Karra, S.; Lemons, N.; Lin, S.; Malyzhenkov, A.; Mascarenas, D.; Mniszewski, S.; Nadiga, B.; O'Malley, D.; Oyen, D.; Pakin, S.; Prasad, L.; Roberts, R.; Romero, P.; Santhi, N.; Sinitsyn, N.; Swart, P. J.; Wendelberger, J. G.; Yoon, B.; Zamora, R.; Zhu, W.; Eidenbenz, S.; Coles, P. J.; Vuffray, M.; Lokhov, A. Y. Quantum algorithm implementations for beginners. https://arxiv.org/abs/1804.03719 (accessed April 9, 2021).

(39) Anon Pennylane. https://pennylane.ai/ (accessed April 9, 2021).

(40) Wang, Y.; Cheng, T.; Bryant, S. H. PubChem BioAssay: A Decade's Development toward Open High-Throughput Screening Data Sharing. *SLAS Discov* **2017**, *22*, 655−666.